Analyst

PAPER

View Article Online
View Journal | View Issue

Cite this: *Analyst*, 2025, **150**, 4621

Detection of CH_4 and SF_6 in small volumes with infrared photoacoustic spectroscopy: A comparison with direct absorption spectroscopy

Ton-Rong Tseng, *[a] Che-Hua Yang, *[a] Hsiao-Chi Lu, [b] Mei-Lin Ho [c] and Bing-Ming Cheng *[b]

Received 22nd June 2025,
Accepted 15th August 2025

DOI: 10.1039/d5an00667h

rsc.li/analyst

Infrared (IR) spectroscopy has been applied to monitor gases in various circumstances; however, the IR spectral technique has limitations in detecting small volumes or trace amounts of gas. To evaluate this issue, we deliberately measured the IR spectra of methane and sulfur hexafluoride using the photoacoustic spectroscopic (PAS) technique for gaseous volumes of 1 mL or less. For comparison, the IR spectra of these gases were also determined by the direct absorption spectroscopy (DAS) method for the same quantities. As results, we found that the IR-PAS technique can compete with DAS with advantages including better baseline, scan time saving, and less distortion from the background for the same quantities of small gaseous samples. The calibrations of the intensity *vs.* absolute amount of gas and the optical path length of the cell were engaged in this work; the results show the relationships are linear, conforming to the successful quantitative analysis for small volumes or minute quantities of gas with the IR-PAS technique. In addition, the IR-PAS spectra of the gases were investigated with various construction materials of sample cells. In this manner, our investigation may further motivate the development of a better means or scheme in the IR-PAS technique for monitoring minute amounts of gas in the future.

Introduction

It is always interesting to develop a cost-effective method for detecting gas for a specific issue or working situation, including environmental monitoring, production control, remote sensing, field measurement, safety and security, emissions from landfill, clinical diagnosis, and biomedical applications.[1–7] To achieve these analytical goals, we usually need to identify and quantify the target gaseous samples. For this purpose, THz systems allow measurements of several gaseous species at the ppm sensitivity level if their rotational spectral lines are widely spaced; also, infrared (IR) spectroscopic methods generally perform with advantages of avoiding the ambiguous problems compared to ones in the visible or ultraviolet region. Especially, a Fourier-transform infrared spectrometer (FTIR) provides a convenient tool in the broad mid-IR region to definitely characterize unknown gases.[8,9] Therefore, it is still of interest to build up a new analytical instrument, scheme or system to improve the well-known techniques based on FTIR for monitoring various gases.

For analysis of gases, we should consider several vital factors, including detectivity, sensitivity, selectivity, application environment, and detection scheme. Among these factors, the amount/volume of the gaseous analyte is an important aspect, which should be considered primarily. Usually, direct absorption spectroscopy (DAS) with a gaseous cell coupled to FTIR provides adequate performance for the analysis of gases. DAS performs better when a large gas cell, potentially equipped with multipath capability, is engaged in the analytical routine. As discussed in a review article,[10] multipath cells such as the White cell, Herriott cell, astigmatic Herriott cell, and the circular gas cell are commonly used to in DAS to achieve low detective limits. These cells extend the optical path lengths but could consequently require larger gaseous volumes. However, the effectiveness of DAS becomes questionable when analysing trace amounts of gaseous samples. Instead, we might need to find an alternative method to overcome the strict requirements for small gaseous samples.

As is well known, photoacoustic spectroscopy (PAS) is a very sensitive scheme for the detection of gases. Therefore, the PAS-based detection system may enable the monitoring of minute gas volumes, in contrast to the larger sample requirements of DAS equipment.[10–15] Using IR light as a source, infrared photoacoustic spectroscopy (IR-PAS) may thus be a workable method for monitoring minute amounts of gases.

[a]*Colledge of Mechanical and Electrical Engineering, National Taipei University of Technology, 1, Sec. 3, Zhongxiao E. Rd., Taipei 10608, Taiwan.*
E-mail: wellsimon@gmail.com, chyang@ntut.edu.tw
[b]*Department of Medical Research, Hualien Tzu Chi Hospital, Buddhist Tzu Chi Medical Foundation, No. 707, Sec. 3, Chung-Yang Rd., Hualien City 970, Taiwan.*
E-mail: bmcheng7323@gmail.com
[c]*Department of Chemistry, Fu Jen Catholic University, New Taipei City 242, Taiwan*

The IR-PAS method has been developed since 1968.[16–21] This technique uses IR light to pump a sample to an excited state and detects the acoustic signal through the nonradiative relaxation process with a detector based on a microphone or a piezoelectric sensor.[22–26] By this means, IR-PAS analyses materials with several advantages including minimal sample preparation, being suitable for opaque materials, and being non-destructive for analytes with modern equipment and light sources. Up to now, the IR-PAS technique has been successfully applied to the analysis of various forms of samples, including gaseous molecules, liquids, solids, and powders.[27–30]

As mentioned above, the IR-PAS technique is assumed to be a suitable candidate for analysing minute gaseous samples. To evidence the potential for analysis, we investigated the IR-PAS detection of CH_4 and SF_6 in small volumes, *e.g.* 1 mL or less. In addition, we also measured those samples in the same quantities using the direct absorption technique for comparison in this work.

Currently, CO_2 plays a critical role in global warming; also, methane acts as an important trace gas for the greenhouse effect in the atmosphere.[31–33] The sources of methane might be leaks from natural gas systems, coal mines, and industrial waste, livestock, and other agricultural ways into air.[34,35] Thus, long-term monitoring of the concentration of CH_4 is of great significance to find the source and sink of CH_4 in various environments. For a better understanding of its impact on global warming and climate change, of industrial practices, and of biomedical applications, people have devoted much effort to real-time and *in situ* measurement of the concentration of CH_4 with high precision and sensitivity. Usually, methane detection methods rely on optical absorption spectroscopy in conjunction with the Beer–Lambert law. In this approach, the amount of light absorbed by methane molecules results in the transmission of light depending on the optical path length and methane concentration. Among these detection methods, laser-based techniques can reach high sensitivity to methane at the ppb level.[36–44] However, these systems usually involve sophisticated operations and complicated constructions. A multipath gas cell coupled to an FTIR spectrometer could also be used to detect methane at the ppb level. Nevertheless, these kinds of arrangements require a large volume of gaseous sample.[45–47] Thus, it is still worth developing the IR-PAS method for monitoring small volumes of methane.

Sulfur hexafluoride, SF_6, is associated with electrical insulation in industrial applications; accidentally, large amounts of SF_6 have leaked into the atmosphere.[48] Unfortunately, SF_6 has thus become a potent greenhouse gas with a steadily increasing atmospheric abundance. Hence, it is also important to develop a new detection method for the analysis of trace amounts of SF_6.

Meanwhile, we did the calibration of the intensity *vs.* the optical path length in an IR-PAS scheme for the first time. The relationship is linear, conforming to the optical configuration. This result implied that the signal of IR-PAS is proportional to the absolute quantity of a gaseous sample. In addition, we studied the PAS signal *vs.* the construction material of the gas cell for future development. Our results provide valuable information on developing inexpensive and portable IR-PAS instruments to monitor minute amounts of gases.

Results and discussion

A gaseous molecule can absorb infrared radiation, which excites it to a higher ro-vibrational state from the ground state. Afterwards, relaxation of the excited state occurs *via* either fluorescence or collisions; generally, the latter process increases the temperature of the gas due to its internal energy transferring to translation. This nonradiative relaxation route happens when the relaxation time can compete with the radiative lifetime in the depopulation of the excited states. Radiative decay has a characteristic lifetime of 10^{-2} s in the mid-IR range. Thus, the decay time of the nonradiative process may be of the order of 10^{-3} s; further, the value depends on the pressure (decay time τ inversely proportional to the pressure). In this work, the scanning speed of the moving mirror of the FTIR system could only be regulated from 0.4 to 1.0 cm s^{-1}. Consequently, the time-dependence of the scanning speed might affect the measured intensity of the nonradiative PAS process and needs to be clarified first.

To visualize the relationship of the signal of the PAS measurement with the scanning speed of FTIR, Fig. 1 displays the IR-PAS spectra of 5000 ppm CH_4/air with a volume of 1 mL at 760 Torr near 298 K recorded with a resolution of 2 cm^{-1} at various scanning speeds: (a) 1.0, (b) 0.8, (c) 0.6, (d) 0.5 and (e) 0.4 cm s^{-1}. Those measured with a resolution of 8 cm^{-1} are shown in Fig. S1 in the SI. In Fig. 1, the vibration-rotational bands of gaseous CH_4 have centers at 1306.7 cm^{-1}, assigned to deformation mode ν_4, and at 3017.4 cm^{-1}, associated with C–H stretching mode ν_3; in the mid-IR region, only these two fundamental modes are regarded as intrinsically active for

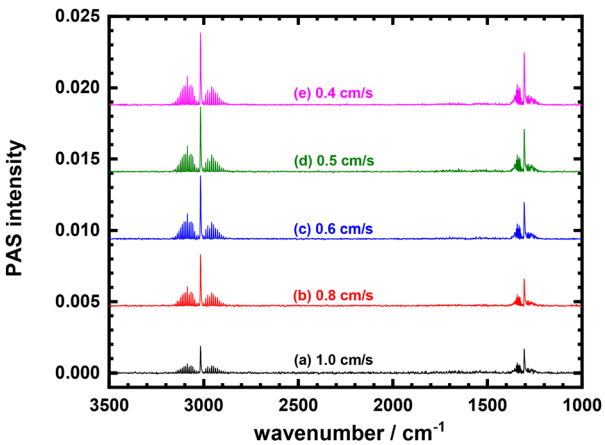

Fig. 1 IR-PAS spectra of 5000 ppm CH_4/air with a volume of 1 mL at 760 Torr near 298 K recorded with a resolution 2 cm^{-1} for various FTIR scanning speeds of (a) 1.0, (b) 0.8 (*Y*-axis offset 0.0047), (c) 0.6 (*Y*-axis offset 0.0094), (d) 0.5 (*Y*-axis offset 0.0141) and (e) 0.4 cm s^{-1} (*Y*-axis offset 0.0188).

methane. Both fundamental vibrational modes involve triply degenerate motions belonging to the symmetry class F in methane.

Based on Fig. 1 and S1, the relationships of the intensities of peaks near 3017 cm^{-1} *vs.* the scanning speed of the moving mirror in the FTIR system at resolutions of 2 and 8 cm^{-1} are displayed in Fig. 2. These relationships are almost linear. As a result, the highest PAS intensities were obtained at a scanning speed of 0.4 cm s^{-1}. For this reason, we conducted the following measurements at this scanning value to obtain the highest intensities of the PAS spectra. For example, Fig. S2 displays the IR-PAS spectra of 5000 ppm CH_4/air recorded at a scanning speed of 0.4 cm s^{-1} with various resolutions (in the SI).

As mentioned above, the IR-PAS spectral signal is due to nonradiative decay after absorption of IR light. In principle, PAS is an indirect form of absorption spectroscopy. Then, it is interesting to compare IR-PAS to DAS. For this purpose, we performed measurements for samples of the same amount of methane using both techniques. Fig. 3(a) shows the IR-PAS spectrum of 5000 ppm CH_4/air with a volume of 1 mL with a resolution 1 cm^{-1} at 760 Torr near 298 K. For comparison, Fig. 3(b) presents the direct absorption spectrum of the same quantity of methane by injecting 1 mL the gas into a 10 cm gaseous cell filled with Ar at 760 Torr near 298 K.

Comparing the overall profile of the PAS spectrum to that of the direct absorption spectrum for methane, we can see that the quality of the former is better than that of the latter in Fig. 3. In the absorption technique, we usually need to run two measurements, one without sample (I_0) and the other with the test gas (I); next, the absorbance (A) of the gas can be derived from eqn (1):

$$A = -\log(I/I_0) = \alpha \cdot b \cdot c \quad (1)$$

in which the parameters α, b, and c represent the absorption cross section of the gas, the optical path length of the cell, and the concentration/number density of the gas, respectively. By this means, the noisy error of the absorption spectrum comes from two measurements (I and I_0) and might be enlarged eventually compared to a single one. In addition, the curve of the baseline might thus be distorted, due to differences in optical or other conditions between the two runs, as shown in Fig. 3(b). Likewise, the absorption spectrum might be inevitably disturbed by the condition in the measurement of I_0. Surely, we could subtract the baseline for the absorption spectrum. However, this kind of subtraction might be artificial and arbitrary sometimes. Subsequently, the subtraction might not always achieve high sensitivity for gas detection. For this reason, we did not apply any subtraction of the background for the DAS spectra in this work. In contrast, PAS directly detects the intensity of the acoustic signal against the excitation wavelength or photon energy only from the gaseous sample. Therefore, PAS does not require running the measurement of the background without a sample and only records the spectrum with the sample once. Consequently, the PAS running scheme may thus benefit from three effects: the first reduces the noise level in the spectrum, the second provides a distortion-free background, and the third can save running time (shortened by half) for measurements under the same resolution and scan numbers.

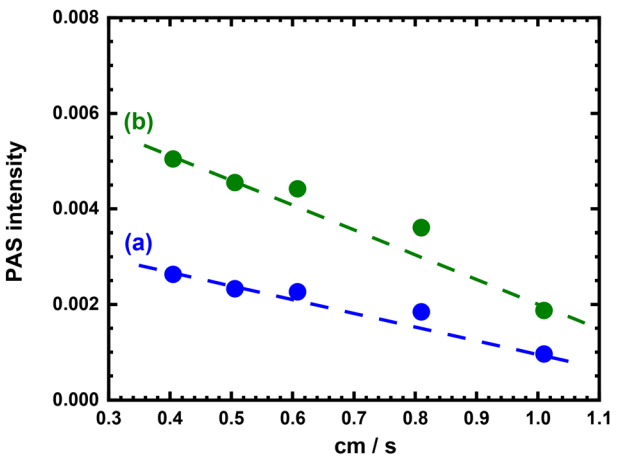

Fig. 2 Relationships of intensities of IR-PAS spectra for peaks at 3017 cm^{-1} *vs.* scanning speed of the moving mirror in the FTIR system for 5000 ppm CH_4/air recorded with resolutions of (a) 8 cm^{-1} and (b) 2 cm^{-1}.

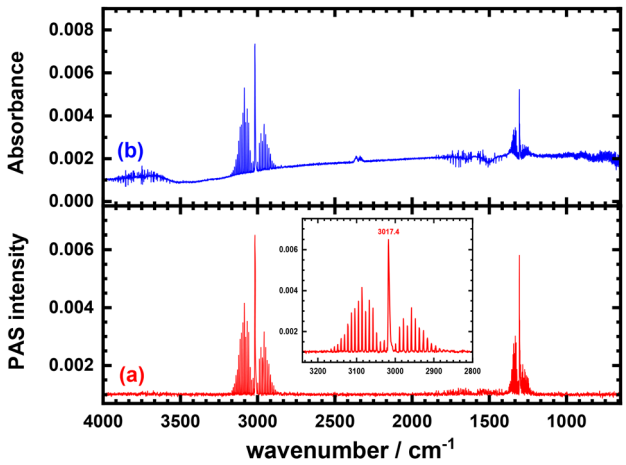

Fig. 3 IR spectra of 5000 ppm CH_4/air recorded with a resolution 1 cm^{-1}. (a) The PAS spectrum for a volume of 1 mL at 760 Torr near 298 K. (b) The direct absorption spectrum for a volume of 1 mL injected into a gaseous Ar cell (10 cm in path length) at 760 Torr near 298 K.

Further, we could compare the detectivities with quantitative values from both spectra. As shown in the inset of Fig. 3(a), the rotational-vibration pattern of the ν_3 mode is well characterized. Accordingly, the signal-to-noise ratio ($R_{(S/N)}$) for the central line at 3017.4 cm^{-1} could be derived to be 180 in the PAS spectrum. Similarly, the value of the ν_3 mode of methane was estimated to be 170 in the absorption spectrum, as shown in Fig. 3(b). However, the spectral quality of the pattern for the ν_4 mode is less than that of the ν_3 mode in the absorption spectrum as displayed in Fig. 3(b). Consequently, the signal-to-noise ratio for the central line at 1305.7 cm^{-1} decreased to 40

in the absorption spectrum. Nonetheless, that ratio still reached a value of 110 in the PAS spectrum.

The detectivity (D) of the sample gas can be estimated from eqn (2):

$$D = Q/R_{(S/N)} \quad (2)$$

where Q represents the absolute quantity of the sample; for the gaseous sample of 5000 ppm CH_4/air, Q is 2.0×10^{-7} mol for a 1 mL volume at 760 Torr and 298 K. Based on the values of $R_{(S/N)}$ for the ν_3 mode, we thus estimated that the detectivities of methane were 1.2×10^{-9} mol for a gaseous volume of 1 mL with both techniques. If we express concentration in terms of ppm, the sensitivities with both methods were 30 ppm for a test volume of only 1 mL. Considering the signals of the ν_4 modes, we derived that the detectivities were 1.8×10^{-9} and 5.0×10^{-9} mol for methane from the PAS and DAS methods, respectively.

In DAS, the absorption is proportional to the absorption cross section of the gas, the optical path length of the cell, and the concentration/number density of the gas, as in eqn (1). Thus, the detectivity depends on the magnitude of the cross section of the gas in the DAS scheme. For this relationship, we would like to verify that the principle still applies in PAS. Considering that the ratio of the IR absorption cross sections of SF_6 to CH_4 is about 20—which is beyond one order of magnitude difference—we subsequently studied SF_6 to obtain additional IR-PAS spectra of this gas. For this purpose, Fig. 4 presents the IR-PAS spectra of 30 ppm SF_6/N_2 near the ν_3 region, 1300–500 cm^{-1}, for a gas volume of 1 mL at 760 Torr near 298 K for various resolutions of 1, 2, 4, and 8 cm^{-1}. The rotation lines of the P, Q, and R branches of the ν_3 band for SF_6 span in the range 940–953 cm^{-1}; in which, the strongest central Q branch is at about 947.2–948.0 cm^{-1} with two weak wings of P and R, the intrinsic linewidths being close to 0.01 cm^{-1}.[49–51] Essentially, the spectral profile of the ν_3 band of SF_6 depends on the temperature, pressure, buffer gas, and resolution measured. Unlike the resolved spectral pattern for methane, the rotational-vibration transitions of the ν_3 mode for gaseous SF_6 present a distinct IR band at 946.6 cm^{-1} at these experimental conditions, as shown in Fig. 4.

For comparison, Fig. 5(a) depicts the IR spectrum of 30 ppm SF_6/N_2 obtained by the PAS technique with a resolution of 1 cm^{-1} at 760 Torr near 298 K for a gas volume of 1 mL, whereas, Fig. 5(b) exhibits that recorded by the direct absorption method for the same quantity of gas, *i.e.* a volume of 1 mL of the gaseous sample injected into a 10 cm gas cell filled with Ar at 760 Torr near 298 K. Accordingly, the signal-to-noise ratio for the ν_3 band of SF_6 at 946.6 cm^{-1} was derived to be about 25 from the PAS spectrum, compared to 18 in the absorption spectrum. Based on the S/N ratios of the ν_3 mode, we thus estimated that the IR detectivities of SF_6 for a gas volume of 1 mL were 4.8×10^{-11} and 6.6×10^{-11} mol (0.048 and 0.066 nmol) with the PAS and absorption techniques, respectively. If we express concentration in terms of ppm, the sensitivities of SF_6 were 1.2 and 1.7 ppm using the PAS and DAS methods, respectively, for a sampling volume of only 1 mL.

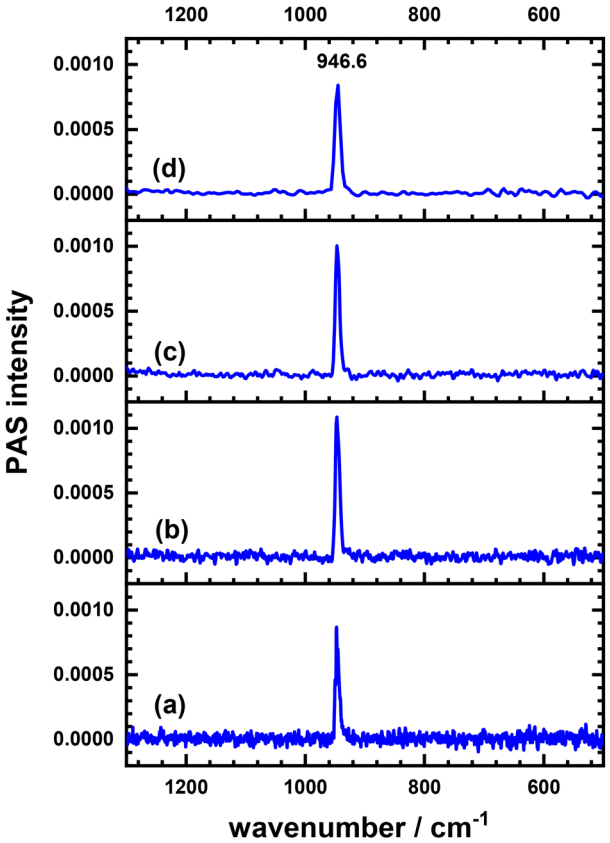

Fig. 4 IR-PAS spectra of 30 ppm SF_6/N_2 for a volume of 1 mL at 760 Torr near 298 K in the wavenumber region 1300–500 cm^{-1} measured with resolutions of (a) 1, (b) 2, (c) 4, and (d) 8 cm^{-1}.

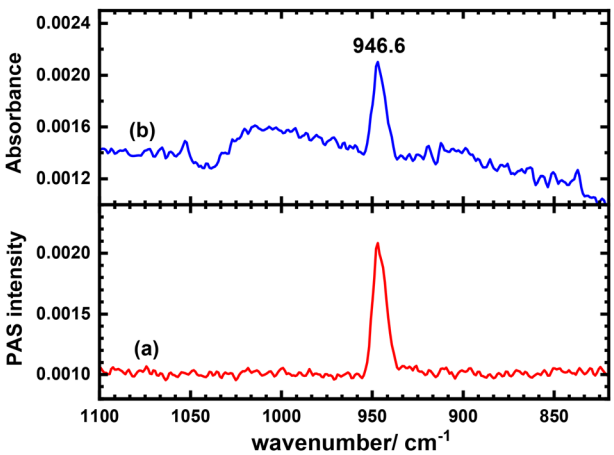

Fig. 5 IR spectra of 30 ppm SF_6/N_2 recorded with a resolution of 1 cm^{-1} near 298 K. (a) The PAS spectrum for a volume of 1 mL at 760 Torr. (b) The absorption spectrum for a volume of 1 mL injected into the gas cell (10 cm path length) filled with Ar at 760 Torr.

Notably, the experimental detectivities of SF_6 and CH_4 were derived to be 0.048 and 1.2 nmol, respectively; thus, the detec-

tivity ratio of SF_6 to CH_4 in the IR-PAS scheme is 25. The value of this ratio for PAS detection is close to the magnitude of the ratio from their absorption cross sections; thus, this result indicates that the detectivity of PAS is similar to that of DAS, depending on the absorption cross section of the gas. Although the detectivities of SF_6 for a volume of 1 mL are comparable in both techniques, the spectral quality of PAS was again better than that of DAS.

In this work, the maximum volume of the gas cell for PAS measurements is 1 mL, which raises the question of the quantitative performance of the IR-PAS method for volumes below 1 mL. To investigate this issue, we performed quantitative tests of SF_6 at volumes less than 1 mL. For this purpose, we determined the IR-PAS spectra of 30 ppm SF_6/N_2 by changing the optical path lengths of the cylindrical gas cell to various values of 11.4, 8.77, 7.95, 7.02, 5.98, 5.02, 4.00, and 2.56 mm corresponding to volumes of 1.00, 0.769, 0.697, 0.616, 0.525, 0.440, 0.351, and 0.225 mL, respectively. Fig. 6 shows the intensities of IR-PAS spectra for 30 ppm SF_6/N_2 *vs.* volume/optical path length recorded with a resolution of 2 cm^{-1} at 760 Torr near 298 K. The signals of the IR-PAS bands varied and depended on the values of volume/optical path length.

According to Fig. 6, the relationship of the PAS peak heights of SF_6 at 946.6 cm^{-1} *vs.* the optical path lengths for 30 ppm SF_6/N_2 at 760 Torr near 298 K is shown in Fig. 7; whereas, Fig. S3 plots the relationship of the intensity of the PAS peak centered at 946.6 cm^{-1} *vs.* the volumes of the gas cell under the same conditions (in the SI). Notably, both relationships are linear within experimental error even when the testing volume is less than 1 mL. In the configuration of the optical system, the signal of IR-PAS is thus directly proportional to the optical path length. The amount of the gaseous molecules is proportional to the volume for the same pressure and temperature. This result demonstrates that the signal of IR-PAS is also proportional to the absolute quantity of gaseous SF_6 in the experimental system. Fig. 7 shows the relationship between the intensity of the PAS peak centered at 946.6 cm^{-1} and the absolute quantity (in units of nmol) of SF_6, recorded at a resolution of 2 cm^{-1} from a 30 ppm SF_6/N_2 sample under 760 Torr near 298 K. The resulting curve is linear.

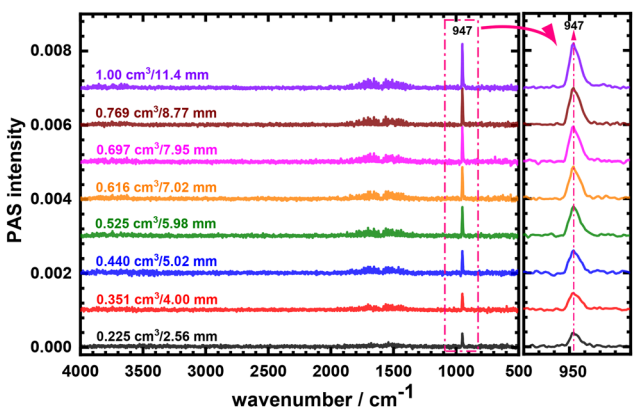

Fig. 6 IR-PAS spectra of 30 ppm SF_6/N_2 measured at various volumes/optical path lengths (*Y*-axis offsets 0.001, respectively) with a resolution of 2 cm^{-1} under 760 Torr near 298 K.

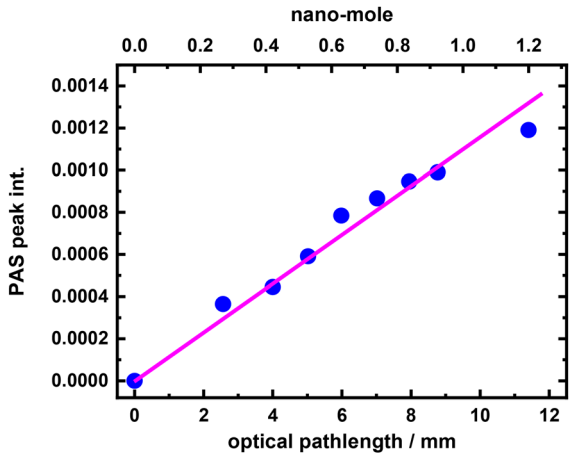

Fig. 7 Relationship of the intensity of the PAS peak centred at 946.6 cm^{-1} *vs.* the optical path length (the lower axis in mm) of the gas cell and absolute quantity (the upper axis in nmol) of SF_6 recorded with a resolution of 2 cm^{-1} from the sample of 30 ppm SF_6/N_2 under 760 Torr near 298 K.

Detectivity can be enhanced by increasing the optical path length, as in multipath-cell designs. Alternatively, optical interaction can be increased by using a hollow-core fibre (HCF) coupled with a laser to achieve a similar goal. As the hollow core is on a micrometer scale, typically, a very small sample is required in the HCF setup.[52–54] Several studies reported that the sensitivity could reach ppb levels using the HCF scheme; unfortunately, the results were not consistent across these works, making it difficult to compare and evaluate the performance of HCF-based sensors.[55–61]

For the above reasons, the gaseous IR-PAS technique remains a promising method for monitoring minute amounts of gases. It does not require an optical detector and possesses high detectivity, allowing measurement of very small gas volumes, potentially less than 1 mL. Based on these advantages, the IR-PAS gas detection technology could be applied to medical diagnosis,[61–64] industrial production,[65–67] environmental monitoring, and other fields.[68,69] Therefore, this technique deserves to be further developed in the future.[70]

To increase the detectivity for the gaseous IR-PAS scheme, we can endeavour to improve the operation, the re-design of the gaseous cell, the selection of a high-response microphone, *etc*. As shown in Fig. 2, the intensities of IR-PAS spectral peaks depend on the scanning speed of the FTIR spectrometer. Specifically, the IR-PAS signal intensity may increase by more than 30% if the FTIR scanning speed is decreased from 0.4 cm s^{-1} to 0.1 cm s^{-1}. Building on this, the detectivity of the IR-PAS spectra can be increased by tuning the FTIR scanning speed.

For monitoring a gas, the sample cell is an indispensable part of the PAS system. In this work, we measured the gaseous IR-PAS spectra using a universal cell (model number LSC001, provided by MTEC Photoacoustic Inc.), which is suitable for

various sample types and might not be specific for a gaseous sample. For this reason, we were interested in enhancing detectivity of the gaseous IR spectra by modifying this universal cell first. Additionally, the acoustic wave could be reflected by the surface of the cell; therefore, the construction of the surface of the cell might influence the PAS signal. To check the surface factor, we made a new similar cell by replacing the copper part of the cup with a gold-plated surface, as shown in the inset of Fig. S4(b) (in the SI). Subsequently, we measured the IR-PAS spectrum of methane using a cell with this gold-plated cup, as shown in Fig. S4(b). As a result, the PAS signal increased by about 30% for the gold-plated surface cup in the cell instead of the original one. Additionally, the noise levels decreased by about one-third for this gold-plated surface cup in the cell. Considering all the advantages, the detectivity of gaseous IR-PAS spectra may increase up to fivefold when using the gold-plated surface cup in the sample cell.

The gas cell of PAS not only contains the gas sample, but also plays an important role in signal collection and signal enhancement making it an important module in the gaseous PAS system. Recently, Xiong *et al.* discussed various kinds of gas cells for the PAS scheme.[70] Their review pointed out that improved photoacoustic cell structures can be effective in reducing the lower limit of gas detection. Therefore, it would be interesting to operate various gas cells for the improvement of the detectivity of the IR-PAS technique in the future.

For this purpose, we first need to study which material is better for making the gas cell. Therefore, we fabricated several removable cups, the shapes of which are the same as the original one shown in the insets of Fig. S4(a), for the gas cell from various materials. Subsequently, we measured the IR-PAS spectra for 5000 ppm CH_4/air with a resolution 2 cm^{-1} under the same conditions. Fig. S5 and S6 display the spectra for metals and polymer materials (in the SI), respectively. The former reveals the spectra using metals: (a) the original cell (Cu), (b) Ti, (c) stainless steel 316 (SS316), (d) iron (Fe), (e) brass (BRA), and (f) Al; the latter presents those using polymers: (a) polyvinyl chloride (PVC), (b) polyoxymethylene (POM), (c) polyetheretherketone (PEEK), and (d) polytetrafluoroethylene (PTFE).

Taking the signal intensity of the ν_3 mode of CH_4 at 3017.4 cm^{-1} from the original cell (Fig. S5(a)) as 100, we normalized other signals and obtained the relative ratios for various metals to be Cu : Ti : SS316 : Fe : BRA : Al = 100 : 94 : 97 : 97 : 103 : 121. We obtained almost the same signals for the cells constructed from the metals copper, titanium, stainless steel 316, iron, and brass in the gaseous IR-PAS measurements. Nevertheless, we enhanced the signal above 20% for the cell made of aluminium. For polymers, the relative intensities of the signals from the cells based on PVC, POM, PEEK, and PTFE are 57, 58, 60, and 83. These values are lower than those from the metal cells. In summary, we conclude that aluminium might be a good material to construct gas cells for the IR-PAS scheme.

We also note that Sakai *et al.* used tunable mid-IR laser direct absorption spectroscopy (TILDAS) to measure the isotopic ratios of $^{18}O/^{16}O$ and $^{13}C/^{12}C$.[71] Accordingly, their method could detect CO_2 at sub-nanomole levels, in a range of 0.3 nmol (equivalent to 0.3 μg $CaCO_3$ and 3.8 ng carbon) to 30 nmol. In our work, we could detect CH_4 and SF_6 with detectivities of 1.2 nmol and 0.048 nmol, respectively, in experiments using IR-PAS. Therefore, the detectivity of our IR-PAS technique is comparable to that of TILDAS. For the gas-phase IR-PAS technique, we will continue to engage in the development of the gas cell for research and applications. We trust that, along with the improvements in this technique, a new generation of high-performance systems can be developed. Thus, it is possible to sensitively detect gases with the IR-PAS technique and analyse the gases to trace levels in the near future. Then, we can eventually identify the isotopic ratios of gases using the IR-PAS scheme. Furthermore, IR-PAS has the potential to become an analytical tool for the successful detection and quantification of multicomponent gaseous species.[72–77]

Conclusions

The spectral scheme of gaseous IR-PAS is an indirect absorption spectroscopic procedure, which detects the nonradiative relaxation process of gaseous molecules after excitation by IR light. This photoacoustic behaviour refers to the phenomenon of converting an IR response to an acoustic signal. In this work, we performed measurements of IR spectra of gases CH_4/air and SF_6/N_2 for small volumes, 1 mL or less, by using the PAS technique. For comparison, the absorption spectra of these gases for the same quantities were also examined by a direct absorption method. Their detectivities were close to those determined from the IR-PAS method. To monitor such small quantities of gas, we thus conclude that the IR-PAS technique can compete with the direct absorption method with advantages, including baseline improvement, time saving and less distortion from the background. Further, we also studied the IR-PAS spectra of the gases with cells constructed from various materials. Our results provide valuable information for the future development of the IR-PAS technique.

Supported by results, our work demonstrates broad applicability of the IR-PAS technique for gas analysis, highlighting potential applications in medical, diagnostic, industrial, environmental fields. Thus, our work positions the IR-PAS technique as a versatile tool, potentially extending its relevance beyond niche research. Hence, this study may inspire further research to develop the IR-PAS tool for monitoring minute amounts of gas.

Experimental

The IR-PAS system was used to measure the gas spectra, utilizing an FTIR spectrometer (ABB, Quebec, Canada, model FTLA2000-104). The PAS accessory equipped with a microphone detector (model number PAC300) was provided by

MTEC Photoacoustic, Inc.[78] A schematic diagram of the IR-PAS measurement set up is shown in Fig. 8(a). To reduce the interference from environmental gases, the FTIR spectrometer, along with its IR beam path, was flushed with 99.99% pure gaseous nitrogen. Gaseous samples were injected into a photoacoustic cell (supplied by MTEC Photoacoustic Inc., part number LSC001) containing a removable brass cup at the bottom, as shown in Fig. 8(b). The cell diameter is 10.6 mm, with an optical path length of 11.4 mm, resulting in a total volume of 1 mL.

For charging the gaseous sample into the cell, the flow rate of the gas was regulated at 5 cc s^{-1} by a flow controller. After charging the gas for about 10 min, we then sealed the gas cell at 760 Torr near 298 K. We measured the pressure with an MKS Baratron pressure meter (model 127 AA, range 1000 Torr) and the temperature with a thermocouple fluctuating within ±0.2 °C. Using this sampling process, we might consume a greater volume of gas. However, we certainly avoided the contamination/pollution problem of the 1 mL gaseous sample from environmental gas for testing purposes. For spectral measurements, we typically recorded 128 scans for the IR-PAS spectra. To test the signal of PAS *vs.* various materials for the gas cell, we used various in-house–fabricated removable cups for the cell with materials including Cu, Ti, stainless steel 316, iron, brass, Al, polyvinyl chloride, polyoxymethylene and polyetheretherketone. Fig. 8(c) displays the one made from copper with a gold-plated surface.

The direct IR absorption spectra of gaseous samples were also recorded with a gas cell attached to the ABB 65 FTLA2000-104 FTIR spectrometer with a KBr beam splitter and a deuterated alanine-doped triglycine sulphate (DTGS) detector (see selected information in section 7 of SI). A schematic diagram for the measurement of the IR DAS spectra is revealed in Fig. S8 (in the SI). The optical path length of the cylindrical gas cell is 10 cm, sealed with two KBr windows. Its radius is 9.5 mm, resulting in a total volume of 28.3 mL. Additionally, the FTIR spectrometer, along with the IR beam path, was purged with high-purity nitrogen gas. Typically, we performed 128 scans of the absorption spectra for both the reference and the sample. The reference spectrum was taken from the gas cell filled with Ar at 760 Torr near 298 K.

The gaseous Ar was obtained from Matheson with a nominal purity of 99.999%. The CH_4/air was purchased from Shenyi Gas Co. Ltd (in Taiwan) with a concentration of 5000 ppm; SF_6/N_2 was supplied by Chiao Tai Gas Co. Ltd (in Taiwan) with a concentration of 30 ppm.

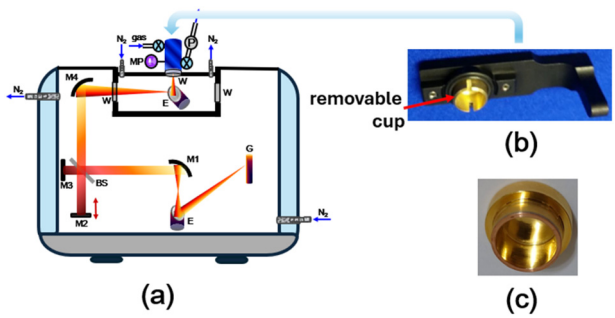

Fig. 8 (a) Schematic diagram for the measurement of gaseous IR spectra with a photoacoustic apparatus. BS: KBr beam splitter; E: ellipsoid; G: globar; M1, M4 and M5: off-axis paraboloid mirrors; M2: scan mirror; M3: flat mirror; MP: microphone; P: pressure meter; W: KBr window. (b) Photograph of the removable brass cup of the gas cell. (c) Photograph of the in-house–fabricated cup from copper with a gold-plated surface.

Author contributions

TRT: conceptualization, data curation, formal analysis, methodology, software, visualization, validation, and writing – original draft. CHY: conceptualization, validation, supervision, and writing – review & editing. HCL: data curation, methodology, formal analysis, writing – original draft. MLH: methodology, validation, writing – review & editing. BMC: project administration, funding acquisition, supervision, and writing – review & editing.

Conflicts of interest

There are no conflicts to declare.

Data availability

All data discussed in this paper will be made available to readers from the corresponding author upon request.

Supplementary information is available. 1. IR-PAS spectra of 5000 ppm CH_4/air recorded with a resolution 8 cm^{-1} *vs.* various scanning speeds of the FTIR; 2. IR-PAS spectra of 5000 ppm CH_4/air recorded with the scanning speed 0.4 cm s^{-1} for the FTIR at various resolutions; 3. relationship of the intensities of the PAS peaks of SF6 centered at 946.6 cm^{-1} *vs.* the volumes of the gas cell; 4. comparison of the IR-PAS spectra of 5000 ppm CH_4/air recorded with the original brass cup in LSC001 cell provided by MTEC Photoacoustic Inc. and the home-made one from copper with gold plated surface; 5. the IR-PAS spectra of 5000 ppm CH_4/air recorded with the removing cup in the gas cell made from various metals; 6. the IR-PAS spectra of 5000 ppm CH_4/air recorded with the removing cup in the gas cell made from various polymers; 7. selected information of the detector in DAS measurement; 8. schematic diagram for the measurement of the DAS spectrum. See DOI: https://doi.org/10.1039/d5an00667h.

Acknowledgements

This work was supported by the National Science and Technology Council of Taiwan with Grant No. NSTC-112-2113-M-303-001.

References

1 A. E. O'Keeffe and G. C. Ortman, *Anal. Chem.*, 1966, **38**, 760–763.
2 D. J. Macfarlane, *Sports Med.*, 2001, **31**, 841–861.
3 G. Atkinson, R. C. R. Davison and A. M. Nevill, *Int. J. Sports Med.*, 2005, **26**, S2–S10.
4 S. Das and M. Pal, *J. Electrochem. Soc.*, 2020, **167**, 037562.
5 E. L. Kerr and J. G. Atwood, *Appl. Opt.*, 1968, **7**, 915–921.
6 L. B. Kreuzer, *J. Appl. Phys.*, 1971, **42**, 2934–2943.
7 A. Sampaolo, P. Patimisco, M. Giglio, A. Zifarelli, H. Wu, L. Dong and V. Spagnolo, *Anal. Chim. Acta*, 2022, **1202**, 338894.
8 P. C. Moura, V. Vassilenko and P. A. Ribeiro, *Emiss. Control Sci. Technol.*, 2023, **9**, 25–46.
9 M. B. Esler, D. W. T. Griffith, S. R. Wilson and L. P. Steele, *Anal. Chem.*, 2000, **72**, 206–215.
10 A. Fathy, Y. M. Sabry, I. W. Hunter, D. Khalil and T. Bourouina, *Laser Photonics Rev.*, 2022, **16**, 2100556.
11 S. Wang, M. Hoffmann, A. K. Yetisen, K. Wang, F. Brändle, W. Kurz and A. W. Koch, *Appl. Spectrosc. Rev.*, 2023, **59**, 382–421.
12 S. Xiong, X. Yin, Q. Wang, J. Xia, Z. Chen, H. Lei, X. Yan, A. Zhu, F. Qiu, B. Chen, Q. Wang, L. Zhang and K. Zhang, *Appl. Spectrosc.*, 2024, **78**, 139–158.
13 C. Chen, Q. Ren and Y. Z. Wang, *Appl. Spectrosc. Rev.*, 2018, **54**, 425–444.
14 R. Selvaraj, N. J. Vasa, S. M. S. Nagendra and B. Mizaikoff, *Molecules*, 2020, **25**, 2227.
15 T. Berer, M. Brandstetter, A. Hochreiner, G. Langer, W. Märzinger, P. Burgholzer and B. Lendl, *Opt. Lett.*, 2015, **40**, 3476–3479.
16 J. F. McClelland, *Anal. Chem.*, 1983, **55**, 89A–105A.
17 G. A. West, J. J. Barrett, D. R. Siebert and K. V. Reddy, *Rev. Sci. Instrum.*, 1983, **54**, 797–817.
18 C. Haisch, *Meas. Sci. Technol.*, 2012, **23**, 012001.
19 P. Patel, M. Hardik and P. Patel, *Int. J. Pharm. Edu.*, 2013, **3**, 41–56.
20 G. Bekiaris, S. Bruun, C. Peltre, S. Houot and L. S. Jensen, *Waste Manage.*, 2015, **39**, 45–56.
21 T. Yang, W. Chen and P. Wang, *Appl. Spectrosc. Rev.*, 2021, **56**, 143–170.
22 E. Max and L. G. Rosengren, *Opt. Commun.*, 1974, **11**, 422–426.
23 P. E. Nordal and S. O. Kanstad, *Opt. Commun.*, 1977, **22**, 185–189.
24 G. Busse and B. Bullemer, *Infrared Phys.*, 1978, **18**, 631–634.
25 M. G. Rockley and J. P. Devlin, *Appl. Spectrosc.*, 1980, **34**, 407–408.
26 D. W. Vidrine, *Appl. Spectrosc.*, 1980, **34**, 314–319.
27 D. C. Dumitras, M. Petrus, A. M. Bratu and C. Popa, *Molecules*, 2020, **25**, 1728.
28 S. N. Thakur, V. N. Rai and J. P. Singh, Chapter 3 - Physics and Techniques of Photoacoustic Spectroscopy of Liquids, in *Photoacoustic and Photothermal Spectroscopy*, ed. S. N. Thakur, V. N. Rai and J. P. Singh, Elsevier, 2023, pp. 51–68.
29 S. J. McGovern, B. S. H. Royce and J. B. Benziger, *Appl. Surf. Sci.*, 1984, **18**, 401–413.
30 B. Ohtani, Photoacoustic Spectroscopy, in *Springer Handbook of Inorganic Photochemistry*, ed. D. Bahnemann and A. O. T. Patrocinio, Springer, Cham, 2022.
31 W. Sun, L. M. J. Kooijmans, K. Maseyk, H. Chen, I. Mammarella, T. Vesala, J. Levula, H. Keskinen and U. Seibt, *Atmos. Chem. Phys.*, 2018, **18**, 1363–1378.
32 K. Butterbach-Bahl, E. M. Baggs, M. Dannenmann, R. Kiese and S. Z. Boltenstern, *Philos. Trans. R. Soc. Lond., B*, 2013, **368**, 20130122.
33 H. Schaefer, S. E. M. Fletcher, C. Veidt, K. R. Lassey, G. W. Brailsford, T. M. Bromley, E. J. Dlugokencky, S. E. Michel, J. B. Miller, I. Levin, D. C. Lowe, R. J. Martin, B. H. Vaughn and J. W. C. White, *Science*, 2016, **352**, 80–84.
34 H. L. Feng, J. H. Guo, M. H. Han, W. F. Wang, C. H. Peng, J. X. Jin, X. Z. Song and S. Q. Yu, *For. Ecol. Manage.*, 2020, **455**, 117702.
35 M. Rigby, R. G. Prinn, P. J. Fraser, P. G. Simmonds, R. L. Langenfelds, J. Huang, D. M. Cunnold, L. P. Steele, P. B. Krummel, R. F. Weiss, S. O'Doherty, P. K. Salameh, H. J. Wang, C. M. Harth, J. Mühle and L. W. Porter, *Geophys. Res. Lett.*, 2008, **35**, L22805.
36 W. Ye, C. Li, C. Zheng, N. P. Sanchez, A. K. Gluszek, A. J. Hudzikowski, L. Dong, R. J. Griffin and F. K. Tittel, *Opt. Express*, 2016, **24**, 16973–16985.
37 L. Shao, B. Fang, X. Qiu, Q. He, J. Wei, C. Li, W. Zhao, *et al.*, *Spectrochim. Acta, Part A*, 2019, **222**, 117118.
38 Y. Yu, N. P. Sanchez, R. J. Griffin and F. K. Tittle, *Opt. Express*, 2016, **24**, 10391–10401.
39 W. Ren, W. Jiang and F. K. Tittle, *Appl. Phys. B*, 2014, **117**, 245–251.
40 J. Kostinek, A. Roiger, K. J. Davis, C. Sweeney, J. P. Digangi, Y. Choi, B. Baier, F. Hase, J. Grob, M. Eckl, T. Klausner and A. Butz, *Atmos. Meas. Tech.*, 2019, **12**, 1767–1783.
41 K. Liu, L. Wang, T. Tan, G. S. Wang, W. J. Zhang, W. D. Chen and X. M. Gao, *Sens. Actuators, B*, 2015, **220**, 1000–1005.
42 H. L. Ma, M. G. Sun, S. B. Zhan, Q. L. Zhang, S. L. Zha, G. S. Wang, K. Liu, M. F. Yi and Z. S. Cao, *Spectrochim. Acta, Part A*, 2020, **226**, 117605.
43 N. Liu, L. Xu, S. Zhou, L. Zhang and J. Li, *ACS Sens.*, 2020, **5**, 3607–3616.
44 J. Xia, C. Feng, F. Zhu, S. Ye, S. Zhang, A. Kolomenskii, Q. Wang, J. Dong, Z. Wang, W. Jin and H. A. Schuessler, *Sens. Actuators, B*, 2021, **334**, 129641.
45 A. Khodabakhsh, V. Ramaiah-Badarla, L. Rutkowski, A. C. Johansson, K. F. Lee, J. Jiang, C. Mohr, M. E. Fermann and A. Foltynowicz, *Opt. Lett.*, 2016, **41**, 2541.
46 K. C. Cossel, E. M. Waxman, I. A. Finneran, G. A. Blake, J. Ye and N. R. Newbury, *J. Opt. Soc. Am. B*, 2017, **34**, 104–129.
47 A. A. Ruth, J. Orphal and S. E. Fiedler, *Appl. Opt.*, 2007, **46**, 3611–3616.
48 J. Harnisch and A. Eisenhauer, *Geophys. Res. Lett.*, 1998, **25**, 2401–2404.

49 J. J. Harrison, *J. Quant. Spectrosc. Radiat. Transfer*, 2020, **254**, 107202.
50 C. Chapados and G. Birnbaum, *J. Mol. Spectrosc.*, 1988, **132**, 323–351.
51 R. Fröchtenicht, J. P. Toennies and A. Vilesov, *Chem. Phys. Lett.*, 1994, **229**, 1–7.
52 M. Nikodem, *Materials*, 2020, **13**, 3983.
53 B. T. Thompson, A. Inberg, N. Croitoru and B. Mizaikoff, *Appl. Spectrosc.*, 2006, **20**, 266–271.
54 N. Kuruba and T. Lu, *Sensors*, 2019, **19**, 806.
55 J. Chen, A. Hangauer, R. Strzoda, M. Fleischer and M.-C. Amann, *Opt. Lett.*, 2010, **35**, 3577–3579.
56 K. Krzempek, K. Abramski and M. Nikodem, *Sensors*, 2019, **19**, 3352.
57 W. Jin, Y. Cao, F. Yang and H. L. Ho, *Nat. Commun.*, 2015, **6**, 6767.
58 B. M. Masum, S. M. Aminossadati, M. S. Kizil and C. R. Leonardi, *Appl. Opt.*, 2019, **58**, 963–972.
59 P. Zhao, Y. Zhao, H. Bao, H. L. Ho, W. Jin, S. Fan, S. Gao, Y. Wang and P. Wang, *Nat. Commun.*, 2020, **11**, 847.
60 D. N. Barreto, V. Kokoric, J. F. da Silveira Petruci and B. Mizaikoff, *ACS Meas. Sci. Au*, 2021, **1**, 97–109.
61 Y. Yan, X. Xiao, Q. Nie, Z. Wang, Y. Chen, J. Wu, N. Zhou, R. Zhou, S. Yang and W. Ren, *Laser Photonics Rev.*, 2024, **18**, 2400907.
62 M. J. Navas, A. M. Jiménez and A. G. Asuero, *Clin. Chim. Acta*, 2012, **413**, 1171–1178.
63 C. Popa, *J. Biomed. Opt.*, 2015, **20**, 051003.
64 C. D. Dan, M. Petrus, A. M. Bratu and C. Popa, *Molecules*, 2020, **25**, 1728.
65 A. J. Schmithausen, M. Trimborn and W. Büscher, *Sensors*, 2016, **16**, 1638.
66 B. AnaMaria, P. Cristina, B. Mihaela and M. Petrus, *Sci. Rep.*, 2021, **11**, 7782.
67 X. Yin, L. Dong, H. Wu, L. Zhang, W. Ma, *et al.*, *Opt. Express*, 2019, **27**, A224–A234.
68 F. G. Linhares, M. A. Lima, G. A. Mothe, M. P. P. de Castro, M. G. da Silva, *et al.*, *Biomass Convers. Biorefin.*, 2019, **9**, 577–583.
69 G. A. Shah, G. M. Shah, M. I. Rashid, J. C. J. Groot, B. Traore, *et al.*, *J. Environ. Manage.*, 2018, **209**, 195–204.
70 S. Xiong, X. Yin, Q. Wang, J. Xia, Z. Chen, H. Lei, X. Yan, A. Zhu, F. Qiu, B. Chen, Q. Wang, L. Zhang and K. Zhang, *Appl. Spectrosc.*, 2024, **78**, 139–158.
71 S. Sakai, T. Otsuka, S. Matsuda, Y. Sakairi, R. Uchida, K. Sugahara, A. Kano and D. Yang, *Anal. Chem.*, 2022, **94**, 6446–6450.
72 J. Li, H. Deng, J. Sun, B. Yu and H. Fischer, *Sens. Actuators, B*, 2016, **231**, 723–732.
73 N. Liu, L. Xu, S. Zhou, L. Zhang and J. Li, *ACS Sens.*, 2020, **5**, 3607–3616.
74 Q. Huang, Y. Wei and J. Li, *Sens. Actuators, B*, 2022, **369**, 132234.
75 L. Xu, S. Zhou, N. Liu, M. Zhang, J. Liang and J. Li, *Anal. Chem.*, 2020, **92**, 14153–14163.
76 X. Tan, H. Zhang, J. Li, H. Wan, Q. Guo, H. Zhu, H. Liu and F. Yi, *Nat. Commun.*, 2020, **11**, 5245.
77 Y. Dong, S. Duan, S. Long, Y. Jiang, X. Ma, *et al.*, *Adv. Funct. Mater.*, 2025, **35**, 2422398.
78 T.-R. Tseng, C.-H. Yang, H.-C. Lu, C.-P. Liu and B.-M. Cheng, *Anal. Chem.*, 2024, **96**, 10732–10737.